

https://doi.org/10.1070/QEL17482

Fast method for computer simulation of luminescence characteristics of multilayer biological tissues with embedded luminescent nanoparticles

D.D. Yakovlev, E.A. Sagaidachnaya, D.A. Yakovlev, V.I. Kochubey

Abstract. **We report a fast and computationally stable method for computer simulation of optical properties of layered scattering systems containing luminescent layers. The method is based on the solution of one-dimensional scalar radiative transfer equations and makes it possible to calculate spectral and angular characteristics of luminescent radiation emerging from the system under various conditions of luminescence excitation. The method is used to estimate the parameters necessary for determining temperature in subcutaneous layers from luminescence spectra of up-conversion nanoparticles embedded in these layers during transcutaneous optical probing.**

Keywords: *photoluminescence, up-conversion nanoparticles, layered scattering medium, biological tissue, computer simulation, thermometry.*

1. Introduction

In many studies, photoluminescence of endogenous components of biological tissues or luminescent agents introduced into the tissue makes it possible to obtain valuable information about the properties and state of the biological object under study, as well as about the processes taking place in it. In *in vivo* macroscopic measurements on biological tissues, a luminescence source (luminescent substance) is usually located in the depth of the sample, and both the exciting radiation and the luminescent radiation on the way from the source to the detector pass through layers of scattering and absorbing tissues. If the scattering and absorption properties of these tissues change significantly depending on the wavelength within the spectral region of the luminescence, then the spectrum of the luminescent radiation emerging from the tissue significantly differs in shape from the luminescence spectrum of the source. In this case, if the luminescence spectrum of the source is informative in the experiment under consideration, then it is necessary to take into account the spectrum transformation of the luminescent radiation when it passes through the biological tissue. In particular, this problem is relevant when using fluorescent nanoparticles for local temperature measurement in biological tissues.

D.D. Yakovlev, E.A. Sagaidachnaya, D.A. Yakovlev Saratov State University, ul. Astrakhanskaya 83, 410012 Saratov, Russia; e-mail: yakovlevday@gmail.com;
V.I. Kochubey Saratov State University, ul. Astrakhanskaya 83, 410012 Saratov, Russia; National Research Tomsk State University, prosp. Lenina 36, 634050 Tomsk, Russia; e-mail: saratov_gu@mail.ru

Received 17 November 2020
Kvantovaya Elektronika **51** (1) 43–51 (2021)
Translated by I.A. Ulitkin

The possibility of using luminescent nanoparticles for local temperature measurement is of great interest in many practical problems of laser medicine and biology [1, 2]. When use is made of nanothermometers, the temperature is determined on the basis of data on the change in intensity [3–5], position, and width of luminescence bands [6], as well as on the intensity ratios of several measured bands. One of the promising types of nanothermometers is up-conversion nanoparticles, which are used to determine the temperature from the ratios of the intensities of the luminescence bands [7]. An example of such nanothermometers is $NaYF_4:Er^{3+},Yb^{3+}$ nanoparticles [8]. Figure 1 shows how the luminescence spectrum of these particles changes (upon excitation at a wavelength of 980 nm) with a change in temperature. If nanoparticles are located deep in biological tissue, for example, under the skin in the subcutaneous fat layer or in muscle tissue, then the temperature measurement in the region of location of nanoparticles from the recorded fluorescence spectra during laser transcutaneous optical probing should take into account the spectrum transformation of the luminescent radiation as it propagates inside the tissue.

To determine the temperature from the luminescence spectrum of up-conversion nanoparticles, we should estimate relations of the form [8]

$$f_p(\lambda_r,\lambda_i) = I_{fp}(\lambda_i)/I_{fp}(\lambda_r),$$

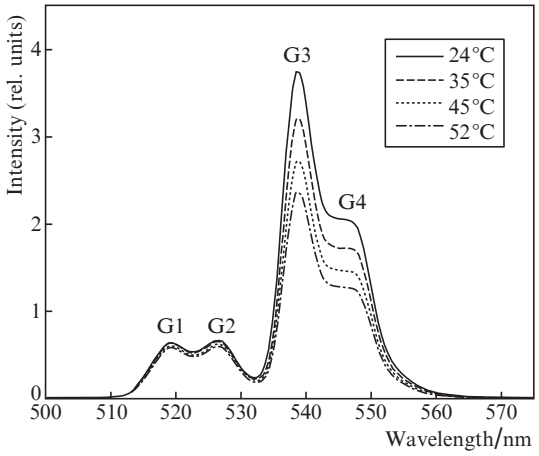

Figure 1. Luminescence spectra of up-conversion $NaYF_4:Er^{3+},Yb^{3+}$ nanoparticles at different temperatures; excitation is performed at a wavelength of 980 nm.

where $I_{fp}(\lambda)$ is the luminescence intensity of nanoparticles at a wavelength λ; λ_r is the wavelength corresponding to one of the spectral maxima of luminescence of nanoparticles; and λ_i ($i = 1, 2, \ldots$) are the wavelengths corresponding to other maxima of the luminescence spectrum of nanoparticles. The parameters $f_p(\lambda_r, \lambda_i)$ are estimated from the measured intensity spectra $I_{ft}(\lambda)$ of the luminescent radiation emerging from the sample by using the expression

$$f_t(\lambda_r, \lambda_i) = I_{ft}(\lambda_i)/I_{ft}(\lambda_r).$$

In the general case, when the scattering and absorption parameters of the tissues through which the luminescent radiation passes on its way to the detector depend on the wavelength, the relationship between the spectra $f_p(\lambda_r, \lambda)$ and $f_t(\lambda_r, \lambda)$ can be expressed as

$$f_t(\lambda_r, \lambda) = a_{tp}(\lambda_r, \lambda) f_p(\lambda_r, \lambda),$$

and a reliable assessment of $f_p(\lambda_r, \lambda_i)$ requires a sufficiently accurate estimate of $a_{tp}(\lambda_r, \lambda_i)$. According to the data given in [8], in the case of determining the temperature from the ratio of the peak intensities of G1 (λ_r = 519 nm, Fig. 1) and G4 bands (λ_3 = 546 nm) with a relative error of 1% in estimating $a_{tp}(\lambda_r, \lambda_3)$, the resulting error in determining the temperature is about 1 °C.

In this paper, we propose a fast and stable calculation method that allows the values of $a_{tp}(\lambda_r, \lambda_i)$ to be calculated for multilayer systems at given scattering and absorption parameters of the layers taking into account multiple scattering (Sections 2–6). Calculations can be performed for both normal and oblique incidence of the exciting radiation on the sample. This method calculates the angular distribution of luminescence radiation emerging from the multilayer system, which makes it possible to quickly compute the values of $a_{tp}(\lambda_r, \lambda_i)$ for different detection angles. Section 7 presents the theoretical estimates of the coefficients $a_{tp}(\lambda_r, \lambda_i)$, obtained using this method, when $NaYF_4:Er^{3+}, Yb^{3+}$ nanoparticles are embedded under the skin in the fat layer and in muscle tissue for different detection angles.

The proposed method is based on the scalar radiative transfer theory. A system of plane-parallel scattering layers is considered as an optical model of the biological tissue. This approach has shown its reliability in solving many optical problems for biological tissues [9–13]. In the numerical solution of problems of the transfer theory for layered systems, algorithms of stochastic tracing of wave packets, based on the Monte Carlo method (MC algorithms) [10, 11, 14–20], the method of discrete ordinates [20–24], and the adding–doubling method (ADM) [10, 11, 25–27] are most widely used. The above approaches are also used to calculate luminescence characteristics of multilayer scattering media [15–20, 22–24, 26, 27]. Stochastic tracing is the most versatile tool, but it requires very large computational resources, which increase with increasing thickness of the system in question. Of these methods, the adding–doubling method is the most computationally efficient, but it is not as versatile as stochastic tracing. One of the disadvantages of the known ADM variants is that they are applicable exclusively for axisymmetric geometry, when the angular radiation spectrum is invariant under any rotation about the normal to the surface of the layered system, which, in particular, does not make it possible to consider a practically interesting case of oblique illumination of the sample by a directed beam. In addition, the use of the doubling procedure for calculating the transmission and reflection operators does not always guarantee the achievement of a high calculation accuracy [25, 28].

The calculation method developed by us is based on the solution of one-dimensional transfer equations in discrete form for radiation with an arbitrary angular distribution (Section 2). To calculate the matrix operators characterising the action of layers with constant (independent of coordinates) scattering and luminescence parameters, we use the mode representation of the radiation characteristics (Section 3). This representation is widely employed in solving radiative transfer problems within the framework of the method of singular eigenfunction expansion [12, 13, 21, 28–32] for the homogeneous linearised Boltzmann equation. The most common approach is based on the representation of phase functions and singular eigenfunctions in the form of expansions in Legendre polynomials (P_N method) [12–14, 21, 28, 31]. In our case, the mode representation is used to solve the radiative transfer equation in a form that is discrete with respect to angular variables. The mode representation allows one to apply a very stable calculation procedure and quickly estimate the characteristics of layers of any thickness, including semi-infinite ones (the computational costs do not depend on the layer thickness) (Section 3), which is one of the main advantages of this representation [28].

The method of discretisation of the transfer equations used by us allows one, in contrast to the P_N method, to consider the case of oblique incidence of a directed light beam on the layered system. When calculating operators for systems of layers from operators for individual layers, an adding technique, similar to that described in [27], is used (Section 4). Operators characterising the transmission of light through interfaces with a sharp jump in the refractive index are calculated using the Fresnel formulae (Section 5), similarly to the ADM algorithm-based procedure proposed by Prahl [11]. A semi-infinite scattering medium (possibly luminescent) can be considered as the last layer of the system.

2. Discrete form of the radiative transfer equation for multilayer luminescent media

2.1. Radiative transfer equation

The proposed calculation method is based on a system of two coupled stationary transfer equations describing the propagation of radiation within a plane-parallel scattering layer with spatially independent parameters of absorption, scattering, and luminescence (homogeneous scattering layer). One of these equations describes the spatial evolution of the radiance I_{ex} of monochromatic exciting radiation with a wavelength λ_{ex} or quasi-monochromatic exciting radiation with a centre wavelength λ_{ex} and an effective spectral range $\Delta\lambda_{ex}$ ($\Delta\lambda_{ex} \ll \lambda_{ex}$) and has the form

$$\boldsymbol{s}\nabla I_{ex}(\boldsymbol{r}, \boldsymbol{s}) = -\mu_{ex\text{-}t} I_{ex}(\boldsymbol{r}, \boldsymbol{s}) + \mu_{ex\text{-}s} \int_{4\pi} p_{ex}(\boldsymbol{s}, \boldsymbol{s}') I_{ex}(\boldsymbol{r}, \boldsymbol{s}') \mathrm{d}\Omega'. \quad (1)$$

Another equation describes the spatial evolution of the radiance I_{fl} of a quasi-monochromatic component of the luminescent radiation, the spectral components of which fill a narrow wavelength range ($\lambda_{fl} - \Delta\lambda_{fl}/2$, $\lambda_{fl} + \Delta\lambda_{fl}/2$) with the centre wavelength λ_{fl}:

$$\boldsymbol{s}\nabla I_{fl}(\boldsymbol{r}, \boldsymbol{s}) = -\mu_{fl\text{-}t} I_{fl}(\boldsymbol{r}, \boldsymbol{s}) + \mu_{fl\text{-}s} \int_{4\pi} p_{fl}(\boldsymbol{s}, \boldsymbol{s}') I_{fl}(\boldsymbol{r}, \boldsymbol{s}') \mathrm{d}\Omega' +$$

$$+ \mu_{\text{ex-a0}} Q \int_{4\pi} f(\boldsymbol{s}, \boldsymbol{s}') I_{\text{ex}}(\boldsymbol{r}, \boldsymbol{s}') \mathrm{d}\Omega'. \quad (2)$$

In these equations, $\mu_{\text{ex-s}}$ and $\mu_{\text{fl-s}}$ are the scattering coefficients at wavelengths λ_{ex} and λ_{fl}, respectively; $\mu_{\text{ex-t}} = \mu_{\text{ex-a0}} + \mu_{\text{ex-a1}} + \mu_{\text{ex-s}}$ and $\mu_{\text{fl-t}} = \mu_{\text{fl-a}} + \mu_{\text{fl-s}}$ are the extinction coefficients at wavelengths λ_{ex} and λ_{fl}; $\mu_{\text{fl-a}}$ is the absorption coefficient at the wavelength λ_{fl}; $\mu_{\text{ex-a0}}$ and $\mu_{\text{ex-a1}}$ are the absorption coefficients, respectively related and unrelated to the excitation of luminescence, at the wavelength λ_{ex}; $p_{\text{ex}}(\boldsymbol{s}, \boldsymbol{s}')$ and $p_{\text{fl}}(\boldsymbol{s}, \boldsymbol{s}')$ are the single scattering phase functions at the wavelengths λ_{ex} and λ_{fl}; $\boldsymbol{s}$ and $\boldsymbol{s}'$ are unit vectors indicating the directions of propagation of the scattered and incident radiation, respectively; $f(\boldsymbol{s}, \boldsymbol{s}')$ is the phase function of photoluminescence; Q is the energy yield of luminescence for the spectral interval $\Delta\lambda_{\text{fl}}$; and $\mathrm{d}\Omega'$ is the solid angle element in the direction of the vector $\boldsymbol{s}'$. The functions $p_{\text{ex}}(\boldsymbol{s}, \boldsymbol{s}')$, $p_{\text{fl}}(\boldsymbol{s}, \boldsymbol{s}')$, and $f(\boldsymbol{s}, \boldsymbol{s}')$ are normalised so that

$$\int_{4\pi} p_{\text{ex}}(\boldsymbol{s}, \boldsymbol{s}') \mathrm{d}\Omega = 1,$$

$$\int_{4\pi} p_{\text{fl}}(\boldsymbol{s}, \boldsymbol{s}') \mathrm{d}\Omega = 1,$$

$$\int_{4\pi} f(\boldsymbol{s}, \boldsymbol{s}') \mathrm{d}\Omega = 1,$$

where $\mathrm{d}\Omega$ is the solid angle element in the direction of the vector $\boldsymbol{s}$.

We will assume that the planes of the layer boundaries of the layered system are parallel to the xy plane of the Cartesian coordinate system xyz. It is also assumed that the layered system is uniformly illuminated. In this case, I_{ex} and I_{fl} in (1) and (2) depend only on z [11, 21], which makes it possible to rewrite these equations in the form

$$\cos\alpha \frac{\mathrm{d}I_{\text{ex}}(z, \boldsymbol{s})}{\mathrm{d}z} = -\mu_{\text{ex-t}} I_{\text{ex}}(z, \boldsymbol{s}) + \mu_{\text{ex-s}} \int_{4\pi} p_{\text{ex}}(\boldsymbol{s}, \boldsymbol{s}') I_{\text{ex}}(z, \boldsymbol{s}') \mathrm{d}\Omega', \quad (3)$$

$$\cos\alpha \frac{\mathrm{d}I_{\text{fl}}(z, \boldsymbol{s})}{\mathrm{d}z} = -\mu_{\text{fl-t}} I_{\text{fl}}(z, \boldsymbol{s}) + \mu_{\text{fl-s}} \int_{4\pi} p_{\text{fl}}(\boldsymbol{s}, \boldsymbol{s}') I_{\text{fl}}(z, \boldsymbol{s}') \mathrm{d}\Omega' + \mu_{\text{ex-a0}} Q \int_{4\pi} f(\boldsymbol{s}, \boldsymbol{s}') I_{\text{ex}}(z, \boldsymbol{s}') \mathrm{d}\Omega', \quad (4)$$

where α is the polar angle of the vector $\boldsymbol{s}$.

2.2. Discretisation of transfer equations

To discretise the transfer equations, a unit sphere of directions is divided into $2M$ elementary cells. The area of the ith cell is denoted by Ω_i. The average irradiances produced by the radiation of this cell are related to the corresponding radiances at the excitation and luminescence wavelengths by the equations:

$$E_{\text{ex}i}(z) = \int_{\Omega_i} I_{\text{ex}}(z, \boldsymbol{s}) |s_z| \mathrm{d}\Omega \approx |\langle s_z \rangle_i| \langle I_{\text{ex}}(z, \boldsymbol{s}) \rangle_i \Omega_i, \quad (5)$$

$$E_{\text{fl}i}(z) = \int_{\Omega_i} I_{\text{fl}}(z, \boldsymbol{s}) |s_z| \mathrm{d}\Omega \approx |\langle s_z \rangle_i| \langle I_{\text{fl}}(z, \boldsymbol{s}) \rangle_i \Omega_i, \quad (6)$$

where angle brackets $\langle ... \rangle_i$ denote averaging over the ith cell and s_z is the z-component of the vector $\boldsymbol{s}$. We replace in (3) and (4) the integration over the solid angle by the summation over cells and, using (5) and (6), write (3) and (4) in the matrix form:

$$\frac{\mathrm{d}\boldsymbol{E}_{\text{fl}}}{\mathrm{d}z} = \boldsymbol{\Delta}_{\text{fl}} \boldsymbol{E}_{\text{fl}} + \boldsymbol{\Delta}_{\text{ex-fl}} \boldsymbol{E}_{\text{ex}}, \quad (7)$$

$$\frac{\mathrm{d}\boldsymbol{E}_{\text{ex}}}{\mathrm{d}z} = \boldsymbol{\Delta}_{\text{ex}} \boldsymbol{E}_{\text{ex}}, \quad (8)$$

where

$$[\boldsymbol{E}_{\text{fl}}]_i = E_{\text{fl}i}; \quad [\boldsymbol{E}_{\text{ex}}]_i = E_{\text{ex}i};$$

$$[\boldsymbol{\Delta}_{\text{fl}}]_{ij} = -\frac{\mu_{\text{fl-t}} \delta_{ij}}{\langle s_z \rangle_i} + \mu_{\text{fl-s}} \frac{\operatorname{sgn}(\langle s_z \rangle_i) \langle \langle p_{\text{fl}}(\boldsymbol{s}, \boldsymbol{s}') \rangle_i \rangle_j \Omega_i}{|\langle s_z \rangle_j|};$$

$$[\boldsymbol{\Delta}_{\text{ex}}]_{ij} = -\frac{\mu_{\text{ex-t}} \delta_{ij}}{\langle s_z \rangle_i} + \frac{\operatorname{sgn}(\langle s_z \rangle_i) \mu_{\text{ex-s}} \langle \langle p_{\text{ex}}(\boldsymbol{s}, \boldsymbol{s}') \rangle_i \rangle_j \Omega_i}{|\langle s_z \rangle_j|};$$

$$[\boldsymbol{\Delta}_{\text{ex-fl}}]_{ij} = \mu_{\text{ex-a0}} Q \frac{\operatorname{sgn}(\langle s_z \rangle_i) \langle \langle f(\boldsymbol{s}, \boldsymbol{s}') \rangle_i \rangle_j \Omega_i}{|\langle s_z \rangle_j|}.$$

2.3. Method for partitioning the unit sphere of directions

A unit sphere of directions is divided into a hemisphere of forward directions and a hemisphere of backward directions. Light fluxes propagating in the direction of the half-space located behind the layered system ($s_z > 0$) will be called forward, while light fluxes propagating in the direction of the half-space located in front of the layered system will be called backward ($s_z < 0$). To describe the propagation of light inside the scattering layers of the layered system, which are assumed to have the same or similar average refractive indices, a basic grid of light propagation directions is introduced, corresponding to a medium with an average refractive index n_{base} of the scattering layers. The basic grid of forward directions is obtained by dividing the unit hemisphere into $M = 4N^2$ (N is an integer) spherical triangles with similar areas (a basic grid for forward radiation at $N = 17$ is shown in Fig. 2). Each elementary spherical triangle represents an elementary cell. The basic grid for backward radiation is the mirror image of the basic grid for forward radiation in the xy plane, with the numbering of the cells being such that the ith grid cell for backward radiation is a mirror image of the ith grid cell for forward radiation. The complete basic grid, which combines the grids for forward and backward radiation, has $2M$ cells, the first M of which correspond to the cells of the basic grid for forward radiation, and the remaining M cells correspond

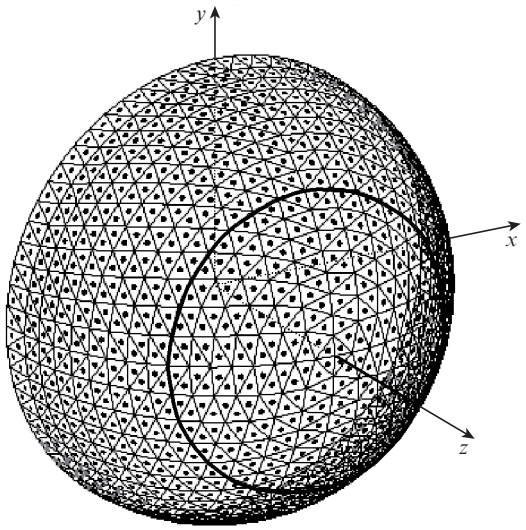

Figure 2. Basic grid for forward radiation.

to the cells of the basic grid for backward radiation. With this cell numbering, the column vectors $\boldsymbol{E}_{\rm fl}$ and $\boldsymbol{E}_{\rm ex}$ entering into Eqns (7) and (8) can be represented as

$$\boldsymbol{E}_{\rm fl} = \begin{pmatrix} \vec{\boldsymbol{E}}_{\rm fl} \\ \overleftarrow{\boldsymbol{E}}_{\rm fl} \end{pmatrix}, \quad \boldsymbol{E}_{\rm ex} = \begin{pmatrix} \vec{\boldsymbol{E}}_{\rm ex} \\ \overleftarrow{\boldsymbol{E}}_{\rm ex} \end{pmatrix},$$

where column vectors with a right arrow characterise the forward propagating radiation, and column vectors with a left arrow characterise the backward propagating radiation.

3. Solution of radiative transfer equations for a homogeneous layer

3.1. General solution

Here, to simplify the formulae, we will assume that the boundary of a homogeneous layer coincides with the plane $z = 0$ and that the layer is located in the half-space $z \geqslant 0$. We represent the vector $\boldsymbol{E}_{\rm ex}$ in the form of a linear combination of normalised eigenvectors $\boldsymbol{\psi}_{{\rm ex}\,j}$ ($\boldsymbol{\psi}_{{\rm ex}\,j}^{\rm T}\boldsymbol{\psi}_{{\rm ex}\,j} = 1$, where the superscript T denotes transposition) of the matrix $\boldsymbol{\Delta}_{\rm ex}$:

$$\boldsymbol{E}_{\rm ex} = \sum_{j=1}^{2M} A_{{\rm ex}\,j}\boldsymbol{\psi}_{{\rm ex}\,j} = \boldsymbol{\Psi}_{\rm ex}\boldsymbol{A}_{\rm ex}, \tag{9}$$

where $\boldsymbol{\Psi}_{\rm ex}$ is a matrix whose columns are vectors $\boldsymbol{\psi}_{{\rm ex}\,j}$,

$$\boldsymbol{\Psi}_{\rm ex} = (\boldsymbol{\psi}_{{\rm ex}\,1}\,\boldsymbol{\psi}_{{\rm ex}\,2}\ldots\boldsymbol{\psi}_{{\rm ex}\,(2M)}),$$

and $\boldsymbol{A}_{\rm ex} = [A_{{\rm ex}\,j}]$ is a $2M$ column vector of the amplitudes $A_{{\rm ex}\,j}$. We will refer to vectors such as $\boldsymbol{E}_{\rm ex}$ as state vectors in the E-representation, and vectors such as $\boldsymbol{A}_{\rm ex}$, as state vectors in the A-representation. Let us rewrite equation (8) using the A-representation:

$$\frac{{\rm d}\boldsymbol{A}_{\rm ex}}{{\rm d}z} = \boldsymbol{\gamma}_{\rm ex}\boldsymbol{A}_{\rm ex}. \tag{10}$$

Here, $\boldsymbol{\gamma}_{\rm ex} = \boldsymbol{\Psi}_{\rm ex}^{-1}\boldsymbol{\Delta}_{\rm ex}\boldsymbol{\Psi}_{\rm ex}$ is a diagonal matrix with elements $[\boldsymbol{\gamma}_{\rm ex}]_{ii} = \gamma_{{\rm ex}\,i}$, where $\gamma_{{\rm ex}\,i}$ is the eigenvalue of the matrix $\boldsymbol{\Delta}_{\rm ex}$, corresponding to the eigenvector $\boldsymbol{\psi}_{{\rm ex}\,i}$. The general solution of equation (10) can be represented as

$$\boldsymbol{A}_{\rm ex}(z) = {\rm e}^{\boldsymbol{\gamma}_{\rm ex}z}\boldsymbol{A}_{\rm ex}(0), \tag{11}$$

where ${\rm e}^{\boldsymbol{\gamma}_{\rm ex}z}$ is a diagonal matrix with elements $[{\rm e}^{\boldsymbol{\gamma}_{\rm ex}z}]_{ii} = {\rm e}^{\gamma_{{\rm ex}\,i}z}$. According to (9) and (11), equation (8) has the following general solution:

$$\boldsymbol{E}_{\rm ex}(z) = \boldsymbol{\Psi}_{\rm ex}{\rm e}^{\boldsymbol{\gamma}_{\rm ex}z}\boldsymbol{\Psi}_{\rm ex}^{-1}\boldsymbol{E}_{\rm ex}(0). \tag{12}$$

Now, similarly to (9), we represent the vector $\boldsymbol{E}_{\rm fl}$ as a linear combination of the normalised eigenvectors $\boldsymbol{\psi}_{{\rm fl}\,i}$ of the matrix $\boldsymbol{\Delta}_{\rm fl}$:

$$\boldsymbol{E}_{\rm fl} = \boldsymbol{\Psi}_{\rm fl}\boldsymbol{A}_{\rm fl},$$

and, using (11), we write (7) in the A-representation:

$$\frac{{\rm d}\boldsymbol{A}_{\rm fl}}{{\rm d}z} = \boldsymbol{\gamma}_{\rm fl}\boldsymbol{A}_{\rm fl} + \boldsymbol{F}{\rm e}^{\boldsymbol{\gamma}_{\rm ex}z}\boldsymbol{A}_{\rm ex}(0), \tag{13}$$

where $\boldsymbol{F} = \boldsymbol{\Psi}_{\rm fl}^{-1}\boldsymbol{\Delta}_{\text{ex-fl}}\boldsymbol{\Psi}_{\rm ex}$; $\boldsymbol{\gamma}_{\rm fl}$ is a diagonal matrix with elements $[\boldsymbol{\gamma}_{\rm fl}]_{ii} = \gamma_{{\rm fl}\,i}$; and $\gamma_{{\rm fl}\,i}$ is the eigenvalue corresponding to the eigenvector $\boldsymbol{\psi}_{{\rm fl}\,i}$. The general solution (13) can be taken in the form

$$\boldsymbol{A}_{\rm fl}(z) = {\rm e}^{\boldsymbol{\gamma}_{\rm ex}z}\boldsymbol{A}_0(0) + \boldsymbol{\Gamma}{\rm e}^{\boldsymbol{\gamma}_{\rm ex}z}\boldsymbol{A}_{\rm ex}(0),$$

where $\boldsymbol{\Gamma}$ is a matrix with elements

$$[\boldsymbol{\Gamma}]_{ij} = \begin{cases} \dfrac{[\boldsymbol{F}]_{ij}}{\gamma_{{\rm ex}\,j} - \gamma_{{\rm fl}\,i}} & \text{at } \gamma_{{\rm ex}\,j} \neq \gamma_{{\rm fl}\,i}, \\ z[\boldsymbol{F}]_{ij} & \text{at } \gamma_{{\rm ex}\,j} = \gamma_{{\rm fl}\,i}. \end{cases}$$

In the E-representation, this solution has the form:

$$\boldsymbol{E}_{\rm fl}(z) = \boldsymbol{\Psi}_{\rm fl}{\rm e}^{\boldsymbol{\gamma}_{\rm ex}z}\boldsymbol{\Psi}_{\rm fl}^{-1}\boldsymbol{E}_0(0) + \boldsymbol{\Psi}_{\rm fl}\boldsymbol{\Gamma}{\rm e}^{\boldsymbol{\gamma}_{\rm ex}z}\boldsymbol{\Psi}_{\rm ex}^{-1}\boldsymbol{E}_{\rm ex}(0). \tag{14}$$

3.2. Algorithm for calculating transmission and reflection matrices for a homogeneous layer

Using the general solution (12), we find expressions for the transmission and reflection matrices of a layer of thickness d. Let us assume that the layer is bounded by the planes $z = z_1$ and $z = z_2$ ($z_2 - z_1 = d$). The transmission matrix $\vec{\boldsymbol{T}}$ [$\vec{\boldsymbol{E}}_{\rm ex}(z_2) = \vec{\boldsymbol{T}}\vec{\boldsymbol{E}}_{\rm ex}(z_1)$ at $\overleftarrow{\boldsymbol{E}}_{\rm ex}(z_2) = \boldsymbol{O}$, where $\boldsymbol{O}$ is the zero vector] and the reflection matrix $\vec{\boldsymbol{R}}$ [$\vec{\boldsymbol{E}}_{\rm ex}(z_1) = \vec{\boldsymbol{R}}\vec{\boldsymbol{E}}_{\rm ex}(z_1)$ at $\overleftarrow{\boldsymbol{E}}_{\rm ex}(z_2) = \boldsymbol{O}$] for radiation incident on the layer from the side $z = z_1$ are derived using the boundary condition $\overleftarrow{\boldsymbol{E}}_{\rm ex}(z_2) = \boldsymbol{O}$, and the transmission matrix $\overleftarrow{\boldsymbol{T}}$ [$\overleftarrow{\boldsymbol{E}}_{\rm ex}(z_1) = \overleftarrow{\boldsymbol{T}}\overleftarrow{\boldsymbol{E}}_{\rm ex}(z_2)$ at $\overleftarrow{\boldsymbol{E}}_{\rm ex}(z_1) = \boldsymbol{O}$] and the reflection matrix $\overleftarrow{\boldsymbol{R}}$ [$\overleftarrow{\boldsymbol{E}}_{\rm ex}(z_2) = \overleftarrow{\boldsymbol{R}}\overleftarrow{\boldsymbol{E}}_{\rm ex}(z_2)$ at $\overleftarrow{\boldsymbol{E}}_{\rm ex}(z_1) = \boldsymbol{O}$] for radiation incident on the layer from the side $z = z_2$ are calculated based on the condition $\vec{\boldsymbol{E}}_{\rm ex}(z_1) = \boldsymbol{O}$. According to (12),

$$\boldsymbol{E}_{\rm ex}(z_2) = \boldsymbol{T}_{\rm ex}(d)\boldsymbol{E}_{\rm ex}(z_1), \quad \boldsymbol{T}_{\rm ex}(d) = \boldsymbol{\Psi}_{\rm ex}{\rm e}^{\boldsymbol{\gamma}_{\rm ex}d}\boldsymbol{\Psi}_{\rm ex}^{-1},$$

where $\boldsymbol{T}_{\rm ex}(d)$ is the $2M \times 2M$ transfer matrix for the layer at the excitation wavelength. There are various methods for calculating transmission and reflection matrices based on such a

representation [28, 32, 33]. It is known that the methods of direct calculation of transmission and reflection matrices for a layer from transfer matrices such as $\boldsymbol{T}_{\rm ex}(d)$ (transfer matrix technique) are numerically unstable at large layer thicknesses [33] because the transfer matrix has very large elements calculated using the elements of the exponential matrix that expotentially grow with increasing d. At layer thicknesses for which the values of these elements become very large, the quantities of interest are given as small differences of very large numbers, which in computer calculations leads to a large loss of accuracy due to the finite word length of the machine. As numerical experiments have shown, when computations are performed with double precision arithmetic, the transfer matrix technique is capable of providing good calculation accuracy only if the value of the largest of the exponential matrix elements does not exceed e^{15}, i.e., the applicability of this technique in our case is limited to the thickness range $d \leqslant 15/\gamma_{\max}$, where $\gamma_{\max}$ is the value of the maximum of $\gamma_{{\rm ex}\,i}$ (for example, in calculations of Section 7 for skin at a wavelength of 519 nm, $\gamma_{\max} = 0.419\ \mu m^{-1}$).

To avoid instabilities in the numerical solution of such problems, somewhat more complex methods are used, in which operations with growing exponents are excluded. Thus, Carroll and Aronson [28] proposed a numerically stable algorithm for calculating the transmission and reflection matrices in the framework of the method of singular eigenfunction expansions using the P_N method. Based on the same principle, we have developed a fairly fast and stable algorithm for calculating transmission and reflection matrices for the problem under consideration. It consists in the following. Since the spectrum of eigenvalues of the transfer equation consists of pairs of eigenvalues equal in magnitude but opposite in sign [13, 21, 28, 31, 32], and in our case, this, in particular, means that the number of positive and negative terms in the set $\{\gamma_{{\rm ex}\,i}\}$ ($i = 1, 2, \ldots, 2M$) is the same, we can number the pairs $\gamma_{{\rm ex}\,i}$ and $\boldsymbol{\psi}_{{\rm ex}\,i}$ so that $\gamma_{{\rm ex}\,i}$ are negative for the first M pairs. With this choice of the eigenmode basis, the vector $\boldsymbol{A}_{\rm ex}$ has the form

$$\boldsymbol{A}_{\rm ex} = \begin{pmatrix} \vec{\boldsymbol{A}}_{\rm ex} \\ \overleftarrow{\boldsymbol{A}}_{\rm ex} \end{pmatrix}, \tag{15}$$

where the vector $\vec{\boldsymbol{A}}_{\rm ex}$ contains the amplitudes $A_{{\rm ex}\,i}$ of mode components with negative $\gamma_{{\rm ex}\,i}$ and characterises the radiation propagating in the $+z$-direction, and the vector $\overleftarrow{\boldsymbol{A}}_{\rm ex}$ characterises the radiation propagating in the $-z$-direction. Having chosen the mode basis in this way, we represent the matrices $\boldsymbol{\Psi}_{\rm ex}$ and $e^{\gamma_{\rm ex} d}$ in block form:

$$\boldsymbol{\Psi}_{\rm ex} = \begin{pmatrix} \boldsymbol{\Psi}_{\rm ex11} & \boldsymbol{\Psi}_{\rm ex21} \\ \boldsymbol{\Psi}_{\rm ex12} & \boldsymbol{\Psi}_{\rm ex22} \end{pmatrix}, \quad e^{\gamma_{\rm ex} d} = \begin{pmatrix} e^{\gamma_{\rm ex+} d} & \boldsymbol{0} \\ \boldsymbol{0} & e^{\gamma_{\rm ex-} d} \end{pmatrix}, \tag{16}$$

where $\boldsymbol{0}$ is a zero matrix. The values of all nonzero elements of the diagonal matrix $\boldsymbol{\gamma}_{\rm ex+}$ are negative, and the values of all nonzero elements of the matrix $\boldsymbol{\gamma}_{\rm ex-}$ are positive. Let us introduce the notation:

$$\begin{aligned} &\boldsymbol{C}_{EA{\rm ex}1} = \boldsymbol{\Psi}_{\rm ex11}^{-1}, \quad \boldsymbol{C}_{EE{\rm ex}1} = \boldsymbol{\Psi}_{\rm ex21}\boldsymbol{\Psi}_{\rm ex11}^{-1}, \\ &\boldsymbol{C}_{AA{\rm ex}1} = \boldsymbol{\Psi}_{\rm ex22} - \boldsymbol{\Psi}_{\rm ex21}\boldsymbol{\Psi}_{\rm ex11}^{-1}\boldsymbol{\Psi}_{\rm ex12}, \\ &\boldsymbol{C}_{AA{\rm ex}1} = -\boldsymbol{\Psi}_{\rm ex11}^{-1}\boldsymbol{\Psi}_{\rm ex12}, \\ &\boldsymbol{C}_{AA{\rm ex}2} = \boldsymbol{\Psi}_{\rm ex11} - \boldsymbol{\Psi}_{\rm ex12}\boldsymbol{\Psi}_{\rm ex22}^{-1}\boldsymbol{\Psi}_{\rm ex21}, \\ &\boldsymbol{C}_{AA{\rm ex}2} = -\boldsymbol{\Psi}_{\rm ex22}^{-1}\boldsymbol{\Psi}_{\rm ex21}, \\ &\boldsymbol{C}_{EA{\rm ex}2} = \boldsymbol{\Psi}_{\rm ex22}^{-1}, \quad \boldsymbol{C}_{EE{\rm ex}2} = \boldsymbol{\Psi}_{\rm ex12}\boldsymbol{\Psi}_{\rm ex22}^{-1}. \end{aligned} \tag{17}$$

Then, in accordance with (12) and the boundary conditions, the matrices $\vec{\boldsymbol{T}}$, $\vec{\boldsymbol{R}}$, $\overleftarrow{\boldsymbol{T}}$, and $\overleftarrow{\boldsymbol{R}}$ can be represented as follows:

$$\vec{\boldsymbol{T}} = \boldsymbol{C}_{AE{\rm ex}2}\vec{\boldsymbol{Y}}_{\rm ex}, \quad \overleftarrow{\boldsymbol{T}} = \boldsymbol{C}_{AE{\rm ex}1}e^{-\gamma_{\rm ex-} d}\vec{\boldsymbol{Y}}_{\rm ex}, \tag{18}$$

$$\begin{aligned} &\vec{\boldsymbol{R}} = \boldsymbol{C}_{EE{\rm ex}1} + \boldsymbol{C}_{AE{\rm ex}1}e^{-\gamma_{\rm ex-} d}\boldsymbol{C}_{AA{\rm ex}2}\,\vec{\boldsymbol{Y}}_{\rm ex}, \\ &\overleftarrow{\boldsymbol{R}} = \boldsymbol{C}_{EE{\rm ex}2} + \boldsymbol{C}_{AE{\rm ex}2}e^{\gamma_{\rm ex+} d}\,\boldsymbol{C}_{AA{\rm ex}1}e^{-\gamma_{\rm ex-} d}\overleftarrow{\boldsymbol{Y}}_{\rm ex}, \\ &\vec{\boldsymbol{Y}}_{\rm ex} = (\boldsymbol{U} - e^{\gamma_{\rm ex+} d}\boldsymbol{C}_{AA{\rm ex}1}e^{-\gamma_{\rm ex-} d}\boldsymbol{C}_{AA{\rm ex}2})^{-1}e^{\gamma_{\rm ex+} d}\boldsymbol{C}_{EA{\rm ex}1}, \\ &\overleftarrow{\boldsymbol{Y}}_{\rm ex} = (\boldsymbol{U} - \boldsymbol{C}_{AA{\rm ex}2}e^{\gamma_{\rm ex+} d}\boldsymbol{C}_{AA{\rm ex}1}e^{-\gamma_{\rm ex-} d})^{-1}\boldsymbol{C}_{EA{\rm ex}2}, \end{aligned} \tag{19}$$

where $\boldsymbol{U}$ is the identity matrix. These formulae have no exponential factors increasing with d, which makes them very convenient and computationally reliable when considering layers of any thickness (see the Appendix). The matrices requiring inversion in expressions (18) and (19) asymptotically approach the identity matrix with increasing d; therefore, their inverses also asymptotically approach the identity matrix with increasing d and retain their stability. None of the matrices that are used in calculations of the transmission and reflection matrices have very large elements in comparison with unity in this case; therefore, no significant loss of accuracy due to rounding caused by the finite word length of the machine occurs when use is made of these formulae. According to (19), the reflection matrix for a layer of infinite thickness (semi-infinite layer) can be calculated by the formula

$$\vec{\boldsymbol{R}} = \boldsymbol{C}_{EE{\rm ex}1}.$$

Similar transmission and reflection operators for luminescent radiation, $\vec{\boldsymbol{t}}$ ($\vec{\boldsymbol{E}}_{\rm fl}(z_2) = \vec{\boldsymbol{t}}\,\vec{\boldsymbol{E}}_{\rm fl}(z_1)$ at $\overleftarrow{\boldsymbol{E}}_{\rm fl}(z_2) = \boldsymbol{O}$), $\vec{\boldsymbol{r}}$ ($\overleftarrow{\boldsymbol{E}}_{\rm fl}(z_1) = \vec{\boldsymbol{r}}\,\vec{\boldsymbol{E}}_{\rm fl}(z_1)$ at $\vec{\boldsymbol{E}}_{\rm fl}(z_2) = \boldsymbol{O}$), $\overleftarrow{\boldsymbol{t}}$ ($\overleftarrow{\boldsymbol{E}}_{\rm fl}(z_1) = \overleftarrow{\boldsymbol{t}}\,\overleftarrow{\boldsymbol{E}}_{\rm fl}(z_2)$ at $\vec{\boldsymbol{E}}_{\rm fl}(z_1) = \boldsymbol{O}$), and $\overleftarrow{\boldsymbol{r}}$ ($\vec{\boldsymbol{E}}_{\rm fl}(z_2) = \overleftarrow{\boldsymbol{r}}\,\overleftarrow{\boldsymbol{E}}_{\rm fl}(z_2)$ at $\overleftarrow{\boldsymbol{E}}_{\rm fl}(z_1) = \boldsymbol{O}$), can be calculated in the same way.

3.3. Algorithm for calculating the luminescence excitation matrices

We will describe the relationship between the fluxes of luminescent radiation emerging from the layer and the flux of exciting radiation when the latter is incident on the layer from the side $z < z_1$ and $z > z_2$ using the excitation matrices $\vec{\boldsymbol{F}}$ ($\vec{\boldsymbol{E}}_{\rm fl} = \vec{\boldsymbol{F}}\vec{\boldsymbol{E}}_{\rm ex}$) and $\vec{\boldsymbol{B}}$ ($\vec{\boldsymbol{E}}_{\rm fl} = \vec{\boldsymbol{B}}\vec{\boldsymbol{E}}_{\rm ex}$) and $\overleftarrow{\boldsymbol{F}}$ ($\overleftarrow{\boldsymbol{E}}_{\rm fl} = \overleftarrow{\boldsymbol{F}}\overleftarrow{\boldsymbol{E}}_{\rm ex}$) and $\overleftarrow{\boldsymbol{B}}$ ($\overleftarrow{\boldsymbol{E}}_{\rm fl} = \overleftarrow{\boldsymbol{B}}\overleftarrow{\boldsymbol{E}}_{\rm ex}$), respectively. The matrices $\vec{\boldsymbol{F}}$ and $\vec{\boldsymbol{B}}$ correspond to the boundary conditions $\vec{\boldsymbol{E}}_{\rm ex}(z_2) = \boldsymbol{O}$, $\vec{\boldsymbol{E}}_{\rm fl}(z_2) = \boldsymbol{O}$, and $\vec{\boldsymbol{E}}_{\rm fl}(z_1) = \boldsymbol{O}$, and the matrices $\overleftarrow{\boldsymbol{F}}$ and $\overleftarrow{\boldsymbol{B}}$ correspond to the boundary conditions $\overleftarrow{\boldsymbol{E}}_{\rm ex}(z_1) = \boldsymbol{O}$, $\overleftarrow{\boldsymbol{E}}_{\rm fl}(z_2) = \boldsymbol{O}$, and $\overleftarrow{\boldsymbol{E}}_{\rm fl}(z_1) = \boldsymbol{O}$. Using the general solution (14), as well as formulae (15)–(17), we can obtain the expressions for these excitation matrices:

$$\vec{\boldsymbol{F}} = \boldsymbol{C}_{AE{\rm fl}2}\vec{\boldsymbol{p}}, \quad \overleftarrow{\boldsymbol{F}} = \boldsymbol{C}_{AE{\rm fl}1}e^{-\gamma_{\rm fl-} d}\vec{\boldsymbol{p}} + \overleftarrow{\boldsymbol{J}}\overleftarrow{\boldsymbol{Y}}_{\rm ex}, \tag{20}$$

$$\vec{\boldsymbol{B}} = \vec{\boldsymbol{L}} + \boldsymbol{C}_{AE{\rm fl}1}e^{-\gamma_{\rm fl-} d}\boldsymbol{C}_{AA{\rm fl}2}\,\vec{\boldsymbol{p}} + \vec{\boldsymbol{J}}\boldsymbol{C}_{AA{\rm ex}2}\vec{\boldsymbol{Y}}_{\rm ex},$$

$$\check{\boldsymbol{B}} = \boldsymbol{C}_{AE\text{fl}2}(\check{\boldsymbol{L}}\check{\boldsymbol{Y}}_{\text{ex}} + \mathrm{e}^{\gamma_{\text{fl}+}d}\boldsymbol{C}_{AA\text{fl}1}\mathrm{e}^{-\gamma_{\text{fl}-}d}\check{\boldsymbol{p}}), \tag{21}$$

where

$$\vec{\boldsymbol{p}} = (\boldsymbol{U} - \mathrm{e}^{\gamma_{\text{fl}+}d}\boldsymbol{C}_{AA\text{fl}1}\mathrm{e}^{-\gamma_{\text{fl}-}d}\boldsymbol{C}_{AA\text{fl}2})^{-1}(\vec{\boldsymbol{J}} + \check{\boldsymbol{L}}\boldsymbol{C}_{AA\text{ex}2}\vec{\boldsymbol{Y}}_{\text{ex}});$$

$$\check{\boldsymbol{p}} = (\boldsymbol{U} - \boldsymbol{C}_{AA\text{fl}2}\mathrm{e}^{\gamma_{\text{fl}+}d}\boldsymbol{C}_{AA\text{fl}1}\mathrm{e}^{-\gamma_{\text{fl}-}d})^{-1}\boldsymbol{C}_{AA\text{fl}2}\check{\boldsymbol{L}}\check{\boldsymbol{Y}}_{\text{ex}};$$

$$\vec{\boldsymbol{J}} = \mathrm{e}^{\gamma_{\text{fl}+}d}\vec{\boldsymbol{q}} + \vec{\boldsymbol{F}}_A\boldsymbol{C}_{EA\text{ex}1}; \quad \check{\boldsymbol{J}} = \boldsymbol{C}_{AE\text{fl}1}\check{\boldsymbol{q}};$$

$$\vec{\boldsymbol{L}} = \boldsymbol{C}_{AE\text{fl}1}\vec{\boldsymbol{B}}_A\boldsymbol{C}_{EA\text{ex}1};$$

$$\check{\boldsymbol{L}} = \check{\boldsymbol{B}}_A + \mathrm{e}^{\gamma_{\text{fl}+}d}\boldsymbol{C}_{AA\text{fl}1}\check{\boldsymbol{q}} + \vec{\boldsymbol{F}}_A\boldsymbol{C}_{AA\text{ex}1}\mathrm{e}^{-\gamma_{\text{ex}-}d};$$

$$\vec{\boldsymbol{q}} = \boldsymbol{C}_{AA\text{fl}1}\vec{\boldsymbol{B}}_A\boldsymbol{C}_{EA\text{ex}1}; \quad \check{\boldsymbol{q}} = \check{\boldsymbol{F}}_A + \vec{\boldsymbol{B}}_A\boldsymbol{C}_{AA\text{ex}1}\mathrm{e}^{-\gamma_{\text{ex}-}d}; \tag{22}$$

$$\vec{\boldsymbol{F}}_A = \boldsymbol{\Gamma}_{11}\mathrm{e}^{\gamma_{\text{ex}+}d} - \mathrm{e}^{\gamma_{\text{fl}+}d}\boldsymbol{\Gamma}_{11}; \quad \vec{\boldsymbol{B}}_A = \boldsymbol{\Gamma}_{21} - \mathrm{e}^{-\gamma_{\text{fl}-}d}\boldsymbol{\Gamma}_{21}\mathrm{e}^{\gamma_{\text{ex}+}d};$$

$$\check{\boldsymbol{F}}_A = \boldsymbol{\Gamma}_{22}\mathrm{e}^{-\gamma_{\text{ex}-}d} - \mathrm{e}^{-\gamma_{\text{fl}-}d}\boldsymbol{\Gamma}_{22}; \quad \check{\boldsymbol{B}}_A = \boldsymbol{\Gamma}_{12} - \mathrm{e}^{\gamma_{\text{fl}+}d}\boldsymbol{\Gamma}_{12}\mathrm{e}^{-\gamma_{\text{ex}-}d};$$

$$\boldsymbol{C}_{AE\text{fl}1} = \boldsymbol{\Psi}_{\text{fl}22} - \boldsymbol{\Psi}_{\text{fl}21}\boldsymbol{\Psi}_{\text{fl}11}^{-1}\boldsymbol{\Psi}_{\text{fl}12}; \quad \boldsymbol{C}_{AA\text{fl}1} = -\boldsymbol{\Psi}_{\text{fl}11}^{-1}\boldsymbol{\Psi}_{\text{fl}12};$$

$$\boldsymbol{C}_{AE\text{fl}2} = \boldsymbol{\Psi}_{\text{fl}11} - \boldsymbol{\Psi}_{\text{fl}12}\boldsymbol{\Psi}_{\text{fl}22}^{-1}\boldsymbol{\Psi}_{\text{fl}21};$$

$$\boldsymbol{C}_{AA\text{fl}2} = -\boldsymbol{\Psi}_{\text{fl}22}^{-1}\boldsymbol{\Psi}_{\text{fl}21};$$

and $\boldsymbol{\Gamma}_{ij}$ are the matrix blocks of

$$\boldsymbol{\Gamma} = \begin{pmatrix} \boldsymbol{\Gamma}_{11} & \boldsymbol{\Gamma}_{12} \\ \boldsymbol{\Gamma}_{21} & \boldsymbol{\Gamma}_{22} \end{pmatrix}.$$

The calculation of the excitation matrices by formulae (20)–(22) is numerically stable, since there are no exponents in the calculations that increase with d, and these formulae can be used for layers of any thickness (in contrast to the expressions for similar operators obtained in [26]). For a semi-infinite layer, the luminescence excitation operator can be calculated by the formula

$$\vec{\boldsymbol{B}} = \boldsymbol{C}_{AE\text{fl}1}\boldsymbol{\Gamma}_{21}\boldsymbol{C}_{EA\text{ex}1}.$$

4. Adding technique for a multi-layer system

The adding technique allows recursively calculating the matrices $\vec{\boldsymbol{T}}, \vec{\boldsymbol{R}}, \vec{\boldsymbol{t}}, \vec{\boldsymbol{r}}, \vec{\boldsymbol{F}}, \vec{\boldsymbol{B}}, \check{\boldsymbol{T}}, \check{\boldsymbol{R}}, \check{\boldsymbol{t}}, \check{\boldsymbol{r}}, \check{\boldsymbol{F}}$, and $\check{\boldsymbol{B}}$ for the entire layered system using the corresponding operators for individual layers. Suppose that for the subsystem consisting of the first n layers, we have calculated a complete set of transmission, reflection, and luminescence excitation operators, $\vec{\boldsymbol{T}}_{(n)}$, $\vec{\boldsymbol{R}}_{(n)}$, $\vec{\boldsymbol{t}}_{(n)}$, $\vec{\boldsymbol{r}}_{(n)}$, $\vec{\boldsymbol{F}}_{(n)}$, $\vec{\boldsymbol{B}}_{(n)}$, $\check{\boldsymbol{T}}_{(n)}$, $\check{\boldsymbol{R}}_{(n)}$, $\check{\boldsymbol{t}}_{(n)}$, $\check{\boldsymbol{r}}_{(n)}$, $\check{\boldsymbol{F}}_{(n)}$, and $\check{\boldsymbol{B}}_{(n)}$, as well as a complete set of such operators for the $n+1$th layer, $\vec{\boldsymbol{T}}_{n+1}$, $\vec{\boldsymbol{R}}_{n+1}$, $\vec{\boldsymbol{t}}_{n+1}$, $\vec{\boldsymbol{r}}_{n+1}$, $\vec{\boldsymbol{F}}_{n+1}$, $\vec{\boldsymbol{B}}_{n+1}$, $\check{\boldsymbol{T}}_{n+1}$, $\check{\boldsymbol{R}}_{n+1}$, $\check{\boldsymbol{t}}_{n+1}$, $\check{\boldsymbol{r}}_{n+1}$, $\check{\boldsymbol{F}}_{n+1}$ and $\check{\boldsymbol{B}}_{n+1}$. By matching the forward and backward radiation fluxes at the boundary between nth and $n+1$th layers (see Section 7.2.2 in [33]), one can obtain the expressions for the operators of the subsystem of $n+1$ layers:

$$\vec{\boldsymbol{T}}_{(n+1)} = \vec{\boldsymbol{T}}_{n+1}\vec{\boldsymbol{M}}_{n+1}, \quad \check{\boldsymbol{T}}_{(n+1)} = \check{\boldsymbol{T}}_{(n)}\check{\boldsymbol{M}}_{n+1}, \tag{23}$$

$$\vec{\boldsymbol{R}}_{(n+1)} = \vec{\boldsymbol{R}}_{(n)} + \check{\boldsymbol{T}}_{(n)}\vec{\boldsymbol{R}}_{n+1}\vec{\boldsymbol{M}}_{n+1},$$

$$\check{\boldsymbol{R}}_{(n+1)} = \check{\boldsymbol{R}}_{n+1} + \vec{\boldsymbol{T}}_{n+1}\check{\boldsymbol{R}}_{(n)}\check{\boldsymbol{M}}_{n+1}, \tag{24}$$

$$\vec{\boldsymbol{t}}_{(n+1)} = \vec{\boldsymbol{t}}_{n+1}\vec{\boldsymbol{l}}_{n+1}, \quad \check{\boldsymbol{t}}_{(n+1)} = \check{\boldsymbol{t}}_{(n)}\check{\boldsymbol{l}}_{n+1}, \tag{25}$$

$$\vec{\boldsymbol{r}}_{(n+1)} = \vec{\boldsymbol{r}}_{(n)} + \check{\boldsymbol{t}}_{(n)}\vec{\boldsymbol{r}}_{n+1}\vec{\boldsymbol{l}}_{n+1},$$

$$\check{\boldsymbol{r}}_{(n+1)} = \check{\boldsymbol{r}}_{n+1} + \vec{\boldsymbol{t}}_{n+1}\check{\boldsymbol{r}}_{(n)}\check{\boldsymbol{l}}_{n+1}, \tag{26}$$

$$\vec{\boldsymbol{F}}_{(n+1)} = \vec{\boldsymbol{t}}_{n+1}\vec{\boldsymbol{m}}_{n+1} + \vec{\boldsymbol{F}}_{n+1}\vec{\boldsymbol{M}}_{n+1}, \tag{27}$$

$$\vec{\boldsymbol{B}}_{(n+1)} = \vec{\boldsymbol{B}}_{(n)} + \check{\boldsymbol{t}}_{(n)}(\vec{\boldsymbol{B}}_{n+1}\vec{\boldsymbol{M}}_{n+1} + \vec{\boldsymbol{r}}_{n+1}\vec{\boldsymbol{m}}_{n+1}) + \check{\boldsymbol{F}}_{(n)}\vec{\boldsymbol{R}}_{n+1}\vec{\boldsymbol{M}}_{n+1}, \tag{28}$$

$$\check{\boldsymbol{F}}_{(n+1)} = \check{\boldsymbol{t}}_{(n)}\check{\boldsymbol{m}}_{n+1} + \check{\boldsymbol{F}}_{(n)}\check{\boldsymbol{M}}_{n+1}, \tag{29}$$

$$\check{\boldsymbol{B}}_{(n+1)} = \check{\boldsymbol{B}}_{n+1} + \check{\boldsymbol{t}}_{n+1}(\check{\boldsymbol{B}}_{(n)}\check{\boldsymbol{M}}_{n+1} + \check{\boldsymbol{r}}_{(n)}\check{\boldsymbol{m}}_{n+1}) + \check{\boldsymbol{F}}_{n+1}\check{\boldsymbol{R}}_{(n)}\check{\boldsymbol{M}}_{n+1}, \tag{30}$$

$$\vec{\boldsymbol{m}}_{n+1} = (\boldsymbol{U} - \check{\boldsymbol{r}}_{(n)}\vec{\boldsymbol{r}}_{n+1})^{-1}(\vec{\boldsymbol{F}}_{(n)} + \check{\boldsymbol{B}}_{(n)}\vec{\boldsymbol{R}}_{n+1}\vec{\boldsymbol{M}}_{n+1} + \check{\boldsymbol{r}}_{(n)}\vec{\boldsymbol{B}}_{n+1}\vec{\boldsymbol{M}}_{n+1}),$$

$$\check{\boldsymbol{m}}_{n+1} = (\boldsymbol{U} - \vec{\boldsymbol{r}}_{n+1}\check{\boldsymbol{r}}_{(n)})^{-1}(\check{\boldsymbol{F}}_{n+1} + \vec{\boldsymbol{B}}_{n+1}\check{\boldsymbol{R}}_{(n)}\check{\boldsymbol{M}}_{n+1} + \vec{\boldsymbol{r}}_{n+1}\check{\boldsymbol{B}}_{(n)}\check{\boldsymbol{M}}_{n+1}),$$

$$\vec{\boldsymbol{M}}_{n+1} = (\boldsymbol{U} - \check{\boldsymbol{R}}_{(n)}\vec{\boldsymbol{R}}_{n+1})^{-1}\vec{\boldsymbol{T}}_{(n)},$$

$$\check{\boldsymbol{M}}_{n+1} = (\boldsymbol{U} - \vec{\boldsymbol{R}}_{n+1}\check{\boldsymbol{R}}_{(n)})^{-1}\check{\boldsymbol{T}}_{n+1},$$

$$\vec{\boldsymbol{l}}_{n+1} = (\boldsymbol{U} - \check{\boldsymbol{r}}_{(n)}\vec{\boldsymbol{r}}_{n+1})^{-1}\vec{\boldsymbol{t}}_{(n)},$$

$$\check{\boldsymbol{l}}_{n+1} = (\boldsymbol{U} - \vec{\boldsymbol{r}}_{n+1}\check{\boldsymbol{r}}_{(n)})^{-1}\check{\boldsymbol{t}}_{n+1}.$$

Expressions similar to (23)–(26) were obtained for nonluminescent media in [11, 33]. Expressions similar to (27) and (28) can be found in [26]. Calculations start from $\vec{\boldsymbol{T}}_{(0)} = \boldsymbol{U}$, $\check{\boldsymbol{R}}_{(0)} = \boldsymbol{0}$, $\vec{\boldsymbol{t}}_{(0)} = \boldsymbol{U}$, $\vec{\boldsymbol{r}}_{(0)} = \boldsymbol{0}$, $\vec{\boldsymbol{F}}_{(0)} = \boldsymbol{0}$, $\vec{\boldsymbol{B}}_{(0)} = \boldsymbol{0}$, $\check{\boldsymbol{T}}_{(0)} = \boldsymbol{U}$, $\check{\boldsymbol{R}}_{(0)} = \boldsymbol{0}$, $\check{\boldsymbol{t}}_{(0)} = \boldsymbol{U}$, $\check{\boldsymbol{r}}_{(0)} = \boldsymbol{0}$, $\check{\boldsymbol{F}}_{(0)} = \boldsymbol{0}$, and $\check{\boldsymbol{B}}_{(0)} = \boldsymbol{0}$; then, reccurence formulae (23)–(30) are used.

5. Operators characterising the interaction of light with interfaces with a sharp jump in the refractive index

The formulae for individual layers given in Sections 3.2 and 3.3 are valid in the case of light incidence from a medium with a refractive index equal to n_{base}. In realistic model systems, as a rule, there is at least one interface with a sharp jump in the refractive index. In the model used in this work (see Section

7), this is the air–scattering medium (skin) interface. To take into account the reflection at such interfaces, the corresponding transmission and reflection operators are used, which are usually calculated using the Fresnel formulae for the transmission and reflection coefficients of an interface (see, for example, [11]). Within the framework of the proposed method, for radiation in air and nonscattering layers with refractive indices different from n_{base}, it is convenient to use grids conjugated with the basic grid, the nodal directions of which are related to the corresponding nodal directions of the basic grid by Snell's law. Let us assume that unit vectors $\boldsymbol{n}_{b0j}$ and $\boldsymbol{n}_{bij}$ ($i = 1, 2, 3$) indicate, respectively, the mean direction and vertices for the jth cell of the basic grid of directions (for layers with a refractive index n_{base}) and $\boldsymbol{n}_{bij} = (x_{bij}, y_{bij}, z_{bij})$ ($i = 0, 1, 2, 3$) in the xyz coordinate system. Then, the corresponding vectors for the jth cell of the conjugate grid for a medium with a refractive index n_s, provided that $n_s > n_{base}$, can be represented as follows:

$$\boldsymbol{n}_{sij} = (x_{sij}, y_{sij}, z_{sij}) = \left(\frac{n_{base}}{n_s} x_{bij}, \frac{n_{base}}{n_s} y_{bij}, \sqrt{1 - \frac{b_{ij}^2}{n_s^2}} \right), \quad (31)$$

where $b_{ij}^2 = n_{base}^2 (x_{bij}^2 + y_{bij}^2)$. For $n_s < n_{base}$, as in the case of air ($n_s = 1$), for some directions $\boldsymbol{n}_{bij}$ the condition

$$b_{ij}^2 > n_s^2 \quad (32)$$

is met. These directions correspond to surface (evanescent) modes in a medium with a refractive index n_s. The cells of the conjugate grid, for all vertices of which condition (32) is satisfied or $b_{ij}^2 = n_s^2$, are considered to be cells of surface modes (the concept of a vertex in this case is conventional). The cells of the conjugate grid, for all vertices of which relation (32) is not satisfied, correspond to the ordinary propagating modes. The vectors $\boldsymbol{n}_{sij}$ for them are calculated by formula (31). The basic grid can always be chosen such that the medium with a given n_s in the conjugate grid has no elementary cells at which both surface and ordinary modes fall. The advantage of using conjugate grids is that the calculation of the transmission and reflection matrices for the interfaces in this case is simple, and the matrices themselves are diagonal. In the calculations of Section 7, the diagonal elements of the transmission matrices, $\vec{\boldsymbol{T}}(\vec{t})$ and $\tilde{\boldsymbol{T}}(\tilde{t})$, and the reflection matrices, $\vec{\boldsymbol{R}}(\vec{r})$ and $\tilde{\boldsymbol{R}}(\tilde{r})$, for the air–scattering medium interface were calculated as the corresponding transmittivities and reflectivities of a plane interface between media with refractive indices $n_s = 1$ and $n_{base} = 1.4$ for unpolarised incident light and directions of its incidence corresponding to the centres of grid cells. This interface was included in the recursive scheme presented in Section 4 as the very first element.

6. Correction for nonlinearity of luminescence excitation

If only one layer is luminescent in the layered system, the solution for luminescent radiation obtained by the method described above can be considered as a solution to the problem of light propagation from a planar source enclosed between non-emitting layers. Properties of this source, the luminosity and the angular dependence of the radiance, can be easily calculated under the given illumination conditions for the system, as well as the radiance of the exciting radiation incident on the luminescent layer and the irradiance of the layer boundaries produced by this radiation. Equation (2) predetermines a linear dependence of the luminescence of the luminescent layer on its irradiance produced by exciting radiation. In the case of up-conversion luminescence, this dependence is more complicated due to the nonlinear dependence of the luminescence power on the power of the exciting radiation [34]. If the optical density of the luminescent layer is low, which is typical for problems associated with the use of up-conversion nanoparticles for thermometry, the nonlinearity of luminescence excitation to a first approximation can be taken into account by changing the luminosity of the luminescent layer in accordance with the specified functional dependence of the luminosity on the irradiance produced by the exciting radiation upon preservation of the angular distribution of the radiance of the luminescent radiation emerging from the layer. Mathematically, within the framework of the method under consideration, such a correction is reduced to a simple renormalisation of the state vectors of the luminescence radiation emerging from the system. The shape of the spectrum of the output luminescence radiation does not change with this correction; therefore, if the final goal of the calculations is to estimate the coefficients $a_{tp}(\lambda_r, \lambda_i)$, there is no need to carry out the correction.

7. Evaluation of correction factors for various locations of fluorescent nanoparticles in the subcutaneous layers

Using the above method, we estimated the degree of transformation of the spectrum shape of luminescent radiation on its way from the luminescence source ($NaYF_4:Er^{3+},Yb^{3+}$ nanoparticles embedded in the subcutaneous layers) to the photodetector. The calculations were performed for the following three-layer model. The first 2-mm-thick layer was a skin model, and the second 0.5-mm-thick layer was a model layer of the subcutaneous adipose tissue. The third layer, considered in the calculations as semi-infinite, served as a model of the muscle tissue. Four variants of location of nanoparticles in the subcutaneous layers were considered. In all four cases, it was assumed that the particles were evenly distributed over a 100 μm thick region: in the first case (variant 1), in the adipose layer in the immediate vicinity of the skin; in the second case (variant 2), in the adipose layer near the muscle layer; and in the third (variant 3) and fourth (variant 4) cases, in the muscle layer at depths from 0.5 mm and from 1 mm, respectively, measured from the lower border of the adipose layer. The single scattering phase functions $p_{ex}(\boldsymbol{s}, \boldsymbol{s}')$ and $p_{fl}(\boldsymbol{s}, \boldsymbol{s}')$ for all layers were taken in the form of the Henyey–Greenstein functions; the fluorescent emission from nanoparticles was considered isotropic [$f(\boldsymbol{s}, \boldsymbol{s}') = 1/4\pi$]. It was assumed that exciting radiation with a wavelength of $\lambda_{ex} = 980$ nm is normally incident on the sample from a medium with a refractive index equal to 1 (air). The coefficients $a_{tp}(\lambda_r, \lambda_i)$ were calculated at $\lambda_r = 519$ nm (G1, Fig. 1), $\lambda_1 = 526$ nm (G2), $\lambda_2 = 538$ nm (G3), and $\lambda_3 = 546$ nm (G4) for detection angles of 5°, 35.6°, and 48.2° (angle between the normal to the outer boundary of the system and the mean direction of propagation of the luminescent radiation entering the photodetector). The values of the absorption (μ_a) and scattering (μ_s) coefficients used in the calculations, as well as the scattering anisotropy factor g at wavelengths of 519, 526, 538, 546, and 980 nm for all three layers are presented in Table 1. The μ_a values for skin and adipose layer correspond to the data given in [35]. The values of g for these two layers were taken

Table 1. Absorption and scattering parameters of the layers used in the calculations.

Layer	Wavelength/nm	μ_a/cm^{-1}	μ_s /cm^{-1}	g
Skin	519	3.33	179.67	0.77
	526	3.27	172.35	0.77
	538	3.18	166.92	0.775
	546	3.13	156.45	0.78
	980	2.48	130.5	0.92
Subcutaneous	519	1.41	457.67	0.97
adipose layer	526	1.42	450.67	0.97
	538	1.44	441.33	0.97
	546	1.4	443	0.97
	980	1.06	378.8	0.975
Muscle tissue	519	1.38	92.33	0.91
	526	1.47	92.09	0.91
	538	1.61	91.69	0.91
	546	1.71	91.42	0.91
	980	0.73	55.14	0.94

from [36, 37], and the μ_s coefficients were calculated from the values of the reduced scattering coefficient μ'_s [35] and the chosen values of g. The data for the muscle layer were taken from [38]. The average refractive index of all layers is taken equal to 1.4. The coefficient $\mu_{ex\text{-}a\,0}$ at $\lambda = 980$ nm in the region of location of nanoparticles is taken equal to 9.2 cm^{-1}. At luminescence wavelengths, the absorption of light by nanoparticles was neglected. In the region of location of nanoparticles, the value of μ_a at $\lambda = 980$ nm was increased by the value of $\mu_{ex\text{-}a\,0}$ relative to the value of μ_a in the region of the layer free of nanoparticles. The assumed values of the energy yield of luminescence $Q(\lambda)$ were as follows: Q(519 nm) = 0.0047, Q(526 nm) = 0.0049, Q(538 nm) = 0.0274, and Q(546 nm) = 0.0151 [at these Q, the relations $f_p(\lambda_r,\lambda_i)$ are close to the experimental ones at a temperature of 24 °C (see Fig. 1), and the quantum yield at a wavelength of 538 nm is $\sim$0.05]. Note that theoretically, the values of $a_{tp}(\lambda_r,\lambda_i)$ should not depend on the choice of $Q(\lambda)$.

The calculation program was written in C#. For algebraic operations with matrices and calculation of eigenvalues and eigenvectors of matrices, it uses the corresponding tools of the Math.Net Numerics library [39]. The calculations were performed using double precision arithmetic. All calculations were performed using the base grid with $N = 12$ (an increase in N for $N \geqslant 12$ did not lead to a significant change in the final results). On a personal computer with a quad-core AMD Ryzen 5 3500U (2.1 GHz) processor, the calculation time for one luminescence wavelength did not exceed 1 min for any of the variants under consideration.

Table 2. Calculated values of the coefficients $a_{tp}(\lambda_r,\lambda_i)$.

Detection angle/deg	i	λ_i/nm	$a_{tp}(\lambda_r,\lambda_i)$			
			variant 1	variant 2	variant 3	variant 4
5	1	526	1.118	1.114	1.098	1.087
	2	538	1.292	1.28	1.236	1.204
	3	546	1.563	1.541	1.463	1.409
35.6	1	526	1.117	1.113	1.098	1.086
	2	538	1.291	1.279	1.235	1.203
	3	546	1.559	1.538	1.46	1.406
48.2	1	526	1.117	1.113	1.098	1.086
	2	538	1.291	1.279	1.235	1.202
	3	546	1.557	1.536	1.458	1.405

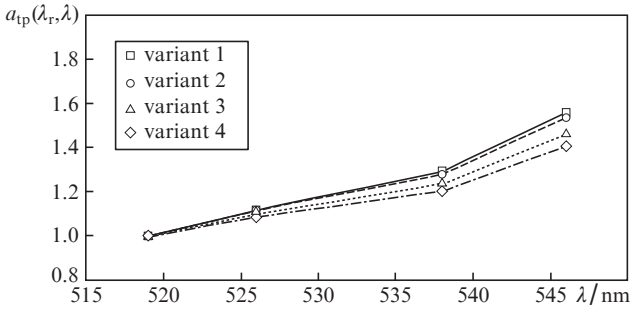

Figure 3. Calculated values of the coefficients $a_{tp}(\lambda_r,\lambda_i)$ for a detection angle of 5°.

The calculation results are shown in Table 2 and Fig. 3. It can be seen from the presented data that in all the cases under study the coefficients $a_{tp}(\lambda_r,\lambda_i)$ differ significantly from 1, despite the closeness of the values of λ_i and λ_r. In this case, the $a_{tp}(\lambda_r,\lambda_i)$ values corresponding to different variants of nanoparticle location differ significantly. At the same time, it can be seen that the course of the $a_{tp}(\lambda_r,\lambda)$ function is mainly determined by the optical properties of the skin. Noteworthy is the fact that the $a_{tp}(\lambda_r,\lambda_i)$ values obtained for different angles of detection differ little from each other. This leads to the idea that in practical measurements under similar conditions the dependence of $a_{tp}(\lambda_r,\lambda_i)$ on the angle of detection in a wide range of its values can be neglected.

8. Conclusions

Thus, we have proposed an efficient and stable method for calculating the characteristics of light fields that arise when light is incident on a layered system containing scattering and luminescent layers. This method is applicable in the case of oblique incidence of the light on the layered medium and is equally effective when considering thin, thick, or semi-infinite layers. The latter distinguishes it favourably from methods of stochastic tracing of wave packets based on the Monte Carlo method, the computational efficiency of which sharply decreases with increasing layer thickness. The proposed method is used to estimate the transformation of the shape of the luminescent radiation spectrum caused by scattering and absorption in the medium, when transcutaneous laser excitation of the luminescence of up-conversion nanoparticles embedded in the subcutaneous layers is performed. The correction factors necessary to determine the temperature from the recorded luminescence spectra were estimated at different locations of nanoparticles in the subcutaneous layers. The presented simulation results make it possible to estimate the error in determining the temperature at different accuracies of localisation of luminescent nanoparticles.

Acknowledgements. The study was supported by the Russian Science Foundation (Project No. 19-12-00118).

Appendix. Program testing results

When testing the software modules for calculating the transmission and reflection operators of homogeneous layers by formulae (18) and (19) (Section 3.2), we compared the results of calculating the integral transmittance (T_{tot}) and reflectance

(R_{tot}) of the scattering layers at normal light incidence by the proposed method with the results obtained using the well-known and widely used version of the adding–doubling method developed by Prahl [11, 40], which are presented in Tables 5.3 and 5.4 of Ref. [40]. We compared the results obtained for layers of media with $g = 0.895$ at $\mu_s/(\mu_s + \mu_a) = 0.6$, 0.9, and 0.99 and the optical thicknesses of the layer, $(\mu_s + \mu_a)d$, from 1 to 512. The calculation by the proposed method was carried out at $N = 12$. In all cases, the absolute difference between the values obtained by these two methods did not exceed 0.015. We also present here for comparison the estimates of T_{tot} and R_{tot} for a 0.02-cm-thick layer of a medium with $\mu_s = 90$ cm^{-1}, $\mu_a = 10$ cm^{-1}, and $g = 0.75$, presented in [11] and [41] (in both cases, Monte Carlo algorithms were employed), and estimates of these quantities obtained by the proposed method for $N = 12$ and 14: $T_{tot} = 0.09711$, 0.09734, 0.09807, 0.09789 and $R_{tot} = 0.66159$, 0.66096, 0.65956, 0.65994 (in the order of mention).

References

1. Gota C., Okabe K., Funatsu T., Harada Y., Uchiyama S. *J. Am. Chem. Soc.*, **131**, 2766 (2009).
2. Yang J.-M., Yang H., Lin L. *ACS Nano*, **5** (6), 5067 (2011).
3. Vetrone F., Naccache R., Zamarrón A., de la Fuente A.J., Sanz-Rodríguez F., Maestro L.M., Rodriguez E.M., Jaque D., Solé J.G., Capobianco J.A. *ACS Nano*, **4** (6), 3254 (2010).
4. Zhao Y., Riemersma C., Pietra F., Koole R., de Mello Donegá C., Meijerink A. *ACS Nano*, **6** (10), 9058 (2012).
5. Labeau O., Tamarat P., Lounis B. *Phys. Rev. Lett.*, **90**, 257404 (2003).
6. Peng H., Stich M.I.J., Yu J., Sun Lining, Fischer L.H., Wolfbeis O.S. *Adv. Mater.*, **22**, 716 (2010).
7. Zengliang Shi et al. *Nanotechnology*, **29**, 094001 (2018).
8. Yanina I.Yu., Volkova E.K., Sagaidachnaya E.A., Kochubey V.I., Tuchin V.V. *Quantum Electron.*, **49**, 59 (2019) [*Kvantovaya Elektron.*, **49**, 59 (2019)].
9. Ishimaru A. *Wave Propagation and Scattering in Random Media* (New York: Acad. Press, 1978; Moscow: Mir, 1981).
10. Tuchin V.V. *Tissue Optics: Light Scattering Methods and Instruments for Medical Diagnosis* (Bellingham, WA: SPIE Press, 2015; Moscow: Fizmatlit, 2013).
11. Prahl S. *PhD Thesis* (University of Texas at Austin, 1988).
12. Phillips K.G., Jacques S.L. *Proc. SPIE*, **7562**, 756207 (2010).
13. Phillips K.G., Jacques S.L. *J. Opt. Soc. Am. A*, **26** (10), 2147 (2009).
14. Meretska M.L., Uppu R., Vissenberg G. *Opt. Express*, **25** (20), A906 (2017).
15. Hughes M.D., Borca-Tasciuc D.-A., Kaminski D.A. *Appl. Opt.*, **55** (12), 3251 (2016).
16. Churmakov D.Y., Meglinsky I.V., Greenhalgh D.A. *J. Biomed. Opt.*, **9** (2), 339 (2004).
17. Churmakov D.Y. Meglinski I.V., Piletsky S.A., Greenhalgh D.A. *J. Phys. D: Appl. Phys.*, **36** (14), 1722 (2003).
18. Dremin V.V., Dunaev A.V. *J. Opt. Technol.*, **83** (1), 43 (2016).
19. Crilly R.J., Cheong W.-F., Wilson B., Spears J.R. *Appl. Opt.*, **36** (25), 6513 (1997).
20. Şahin D., Ilan B. *J. Opt. Soc. Am. A*, **30** (5), 813 (2013).
21. Case K.M., Zweifel P.F. *Linear Transport Theory* (Addison-Wesley: Reading (MA), 1967; Moscow: Mir, 1972).
22. Ma Y., Wang M., Sun J., Hu R., Luo X. *Opt. Express*, **26** (13), 16442 (2018).
23. Joshi A., Rasmussen J.C., Sevick-Muraca E.M., Wareing T.A., McGhee J. *Phys. Med. Biol.*, **53** (8), 2069 (2008).
24. Klose A.D., Hielscher A.H. *Opt. Lett.*, **28** (12), 1019 (2003).
25. Wiscombe W.J. *J. Quant. Spectrosc. Radiat. Transfer*, **18** (2), 245 (1977).
26. Leyre S. et al. *Opt. Express*, **20** (16), 17856 (2012).
27. Leyre S., Cappelle J., Durinck G. *Opt. Express.*, **22** (103), A765 (2014).
28. Caroll G., Aronson R. *Nucl. Sci. Eng.*, **51** (2), 166 (1973).
29. Aronson R., Yarmush D.L. *J. Math. Phys.*, **7** (2), 221 (1966).
30. Aronson R. *Astrophys. J.*, **177**, 411 (1972).
31. Sanchez R., McCormick N.J. *Nucl. Sci. Eng.*, **80** (4), 481 (1982).
32. Aronson R. *Nucl. Sci. Eng.*, **27** (2), 271 (1967).
33. Yakovlev D.A., Chigrinov V.G., Kwok H.-S. *Modeling and Optimization of LCD Optical Performance* (Chichester: Wiley, 2015).
34. Suyver J.F., Aebischer A., García-Revilla S., Gerner P., Güdel H.U. *Phys. Rev. B*, **71**, 125123 (2005).
35. Bashkatov A.N., Genina E.A., Kochubey V.I., Tuchin V.V. *J. Phys. D: Appl. Phys.*, **38**, 2543 (2005).
36. Van Germert M.J.C., Jaques S.L., Sterenborg H.J.C.M., Star W.M. *IEEE Trans. Biomed. Eng.*, **36**, 1146 (1989).
37. Jacques S.L. *Phys. Med. Biol.*, **58**, R37 (2013).
38. Nilsson A.M.K., Berg R., Andersson-Engels S. *Appl. Opt.*, **34**, 4609 (1995).
39. Ruegg C., Cuda M., van Gael J. *Math. Net Numerics* (2016); http://numerics.mathdotnet.com.
40. Prahl A.S., in *Optical-Thermal Response of Laser-Irradiated Tissue* (New York: Springer, 1995) p. 101.
41. Wang L., Jacques S.L. *Monte Carlo Modeling of Light Transport in Multi-layered Tissues in Standard C* (Texas: University of Texas, M.D.Anderson Cancer Center, 1992).